ORIGINAL ARTICLE

Research on the Influence of Multiple Parameters on the Responses of a B-type Subway Train

Yanwen Liu[1,2], Bing Yang[1], Shoune Xiao[1*], Tao Zhu[1], Guangwu Yang[1] and Ruixian Xiu[3]

Abstract

To obtain improved comprehensive crashworthiness criteria for a B-type subway train, the influence laws of the vehicle design collision weight M and empty stroke D on the train's collision responses were investigated, and multi-objective optimization and decision-making were performed to minimize TS (total compression displacement along the moving train) and $TAMA$ (the overall mean acceleration along the moving train). Firstly, a one-dimensional train collision dynamics model was established and verified by comparing with the results of the finite element model. Secondly, based on the dynamics model, the influence laws of M and D on the collision responses, such as the energy-absorbing devices' displacements and absorbed energy, vehicles' velocity and acceleration, TS, $TAMA$ and the coupling correlation effect were investigated. Then, surrogate models for TS and $TAMA$ were developed using the optimal Latin hypercube method (OLHD) and response surface method (RSM), and multi-objective optimization was conducted using the particle swarm optimization algorithm method (MPOSO). Finally, the entropy method was used to obtain the weight coefficients for TS and $TAMA$, and multi-objective decision-making was performed. The results indicate that D and M significantly affect the compression displacements and energy absorption of the first three collision interfaces, but have limited impact on the last three collision interfaces. The velocity versus time curves of vehicle M1 and M2 are shifted and parallel with different D. However, the velocity versus time curves of all the vehicles are shifted but gradually divergent with different M. The maximum collision instantaneous accelerations of the vehicles are directly determined by M, but are only slightly affected by D. Under the coupling effect, all concerned collision responses are strongly correlated with M; however, the responses are weakly correlated with D except for the compression displacement at the M2-M3 collision interface and the maximum collision instantaneous acceleration of vehicle M2. The comprehensive crashworthiness criteria of the B-type subway train were significantly improved after multi-objective optimization and decision-making. The research provides more theoretical and engineering application references for the subway train crashworthiness design.

Keywords: Train collision response, Multi-body dynamics model, Experiment design, Surrogate model, Multi-objective optimization, Entropy method, Multi-objective decision-making

1 Introduction

The crashworthiness of a train is the last barrier to protect the lives of the crew and passengers, and this assessment has become a mandatory requirement in Europe and North America [1–3]. Owing to the characteristics of long marshaling and heavy weight, the enormous kinetic energy transferred during a train collision causes plastic deformation of the vehicle structure and at the same time

*Correspondence: snxiao@swjtu.edu.cn

[1] State Key Laboratory of Traction Power, Southwest Jiaotong University, Chengdu 610031, China

Full list of author information is available at the end of the article

Liu *et al. Chinese Journal of Mechanical Engineering*   (2022) 35:85

Page 2 of 18

generates impact acceleration, resulting in injury or death to the occupants [4]. Maintaining as much structural integrity as possible after the first collision of a train or vehicle, reducing impact acceleration and mitigating secondary collisions of occupants and the vehicle's internal structure are important measures to ensure the safety of occupants and passengers [5, 6].

The research methods used to assess a train's crashworthiness can be divided into theoretical analysis, experimental studies and numerical simulation. Lu [7] established train collision equations based on linear theory assumptions, and studied the influence laws of different vehicles marshaling on the first peak force of the train collision interfaces. According to the simulation results of five different projects, theoretical equations for energy absorption requirements at the front and middle ends of the train were presented. While the theoretical analysis method is usually suitable for simple and linear models, it is very difficult to solve large deformation and nonlinear problems. The experimental studies method can most realistically reflect the crashworthiness characteristics of structures and is favored by many researchers [8–11], but it is expensive and has poor repeatability. The experimental studies method is usually only employed for energy-absorbing devices or small structures, and is not a realistic option for studying the crashworthiness of the entire train. Numerical simulations can compensate for the shortcomings of theoretical analysis and experimental research, and with the maturity of commercial software, this method has been rapidly developed and applied in recent years. Numerical simulation methods include the finite element method and the multi-body dynamics method [4]. Xie et al. [12, 13] investigated the collision responses of two colliding trains and vehicles impacting obstacles using the finite element method respectively. Compared with the finite element method, the multi-body dynamics method can significantly shorten the calculation time, and the calculation accuracy is within the acceptable range in engineering. The multi-body dynamics method has been widely used to study train collision laws and parameter optimization design [14–18].

A great deal of research has been carried out by domestic and international scholars around the crashworthiness of trains. The research conducted in different fields can be summarized as follows. At a global level, the collision response and energy management of the marshaling train have been studied, including the energy-absorption structure distribution and energy-absorbing order optimization [19]; furthermore, cab and interior structure optimization, and occupant secondary collision damage assessments have been conducted [20–24]. At a local level, based on the maximum energy absorption

guideline, special energy-absorption devices have been designed to optimize and improve the energy-absorbing performance [25–30].

The vehicle design collision weight M and train collision speed V are two key factors that significantly affect the train collision behavior [7]. However, only few related studies in the literature have investigated their influence laws on the train collision response. Meanwhile, it has been observed in Ref. [31] that the empty stroke D (the running stroke of the train after the semi-automatic coupler shearing off but before the anti-climber devices contacting) has a clear impact on the compression stroke of the energy-absorbing devices at different collision interfaces. In this study, a typical six-car marshaling B-type subway train is considered as the research object, and a one-dimensional train collision dynamics model is established. Next, the train's comprehensive crashworthiness criteria of *TS* (total compression displacement along the moving train) and *TAMA* (the overall mean acceleration along the moving train) are defined. Then, the influence laws of D and M on the train collision response and the correlation of the coupling effect under the standard collision condition ($V = 25$ km/h) [1] are investigated. Based on the optimal Latin hypercube method (OLHD) and the response surface method (RSM), surrogate models for *TS* and *TAMA* are established, and multi-objective optimization is performed using the particle swarm optimization algorithm (MPOSO). Furthermore, the entropy method is used to obtain the weight coefficients for *TS* and *TAMA* and multi-objective decision-making is performed.

2 Typical B-type Subway Train and Energy-absorbing Devices

The layout of typical energy-absorbing devices of a B-type subway train consisting of six cars is shown in Figure 1. Considering three cars as a basic unit, the overall arrangement is symmetrical. The semi-automatic coupler and anti-climbing energy-absorption devices (anti-climbers) are located at the front end of the lead vehicle. At the collision interfaces between the head vehicle and second vehicle, a semi-permanent coupler A-B is arranged. The semi-permanent coupler C-D is located at the other collision interfaces. The anti-climbing energy-absorption devices are metal cutting-style tubes. The semi-automatic and semi-permanent couplers are combined structures constituting of a rubber buffer and expandable crush tubes.

Figure 2 shows the structure and mechanical characteristics of the energy-absorption devices. All couplers have the same coupler buffer performance with a compression stroke of 73 mm and maximum resistance force of 800 kN. The semi-automatic coupler is equipped

Figure 1 Energy absorption devices and layout of a typical B-type subway train

Figure 2 Energy-absorbing structure and mechanical characteristics: **a** energy-absorption devices, **b** semi-automatic coupler and anti-climber devices, **c** semi-permanent coupler A-B, and **d** semi-permanent coupler C-D
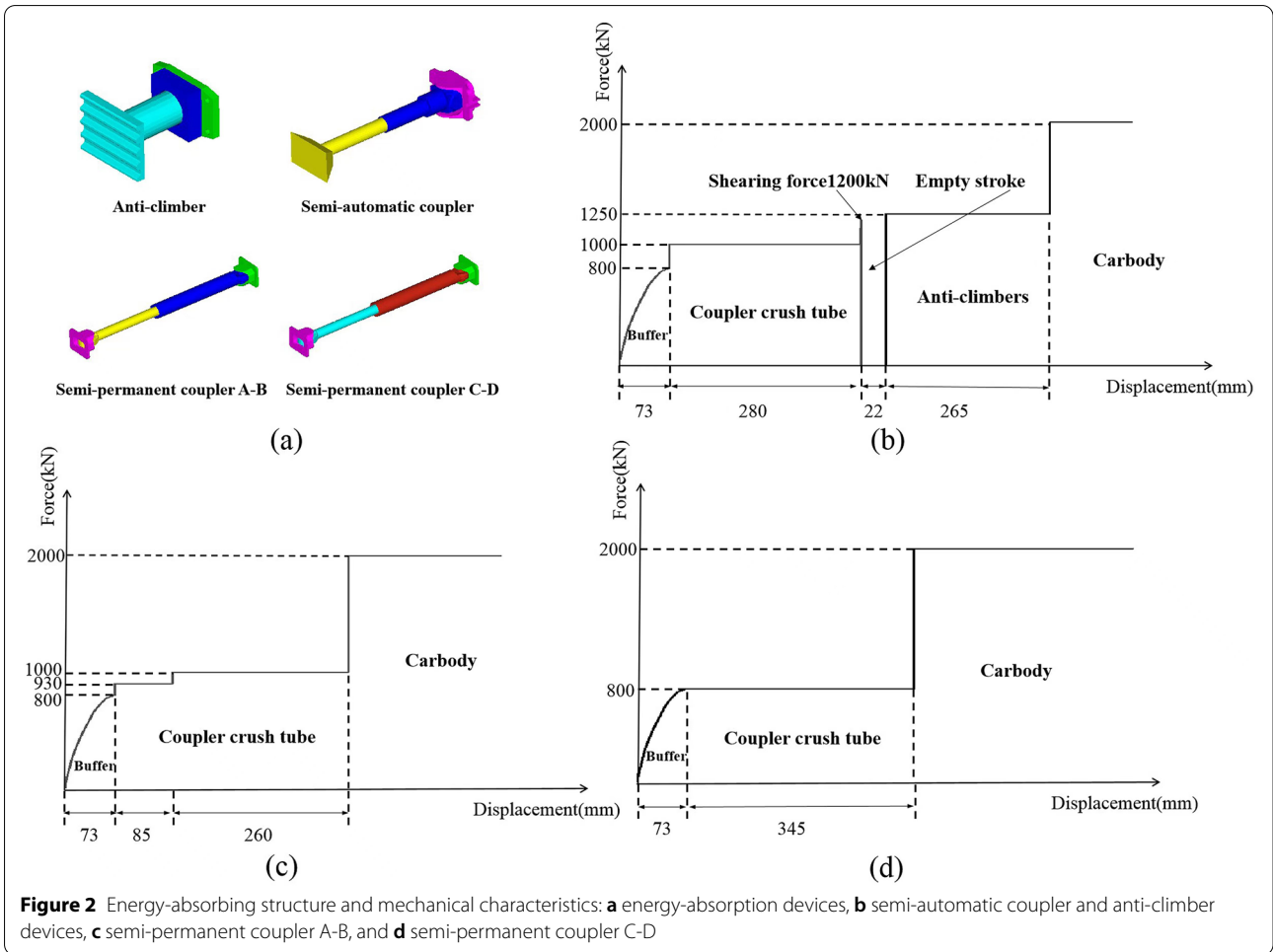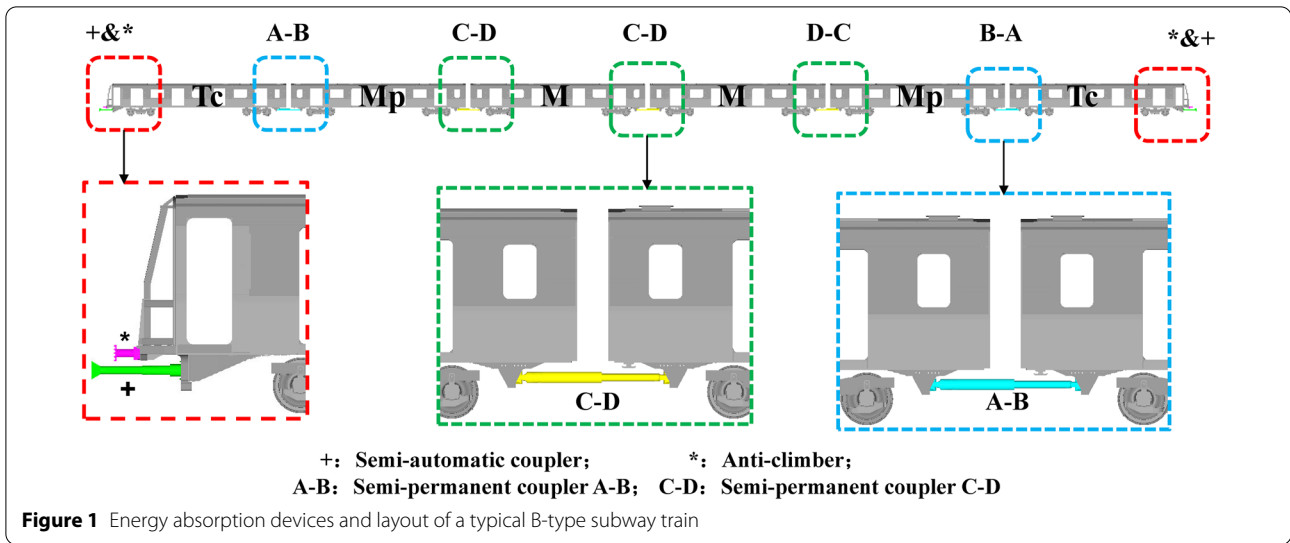
with a shear protection device, and the shearing force is 1200 kN.

After the semi-automatic coupler has been sheared off, the train runs with 22 mm of empty travel, after which

the anti-climbing device makes contact and engages. The average crushing force of the anti-climbing energy-absorption devices is 1250 kN (including two at the head car, each one is 625 kN). The semi-permanent couplers have no shear protection. The crush tubes of the semi-permanent coupler A-B consist of two parts with crushing force of 930 kN and 1000 kN. The crush tubes of the semi-permanent coupler C-D have a crushing force of 800 kN. It is assumed that the equivalent collapsing force of the carbody is 2000 kN.

3 One-dimensional Train Collision Dynamics Model

3.1 Model Building
A one-dimensional train collision dynamics model was formulated using the LS-DYNA software, as shown in Figure 3(a). M1 to M6 and S1 to S6 represent the first to the sixth vehicle of the moving and stationary trains respectively. The train collision dynamics model only considers the degree of freedom in the train's direction of movement.

The modeling method used for the one-dimensional train collision dynamics model is listed in detail in Table 1. The weight of the carbody and bogie is equivalent to the same mass block with #MAT 20 material, and only the degree of freedom in the moving direction of the train is retained. The weight of the vehicle can be changed by adjusting the material's density. The anti-climbing energy-absorption devices, semi-automatic couplers and semi-permanent couplers are simulated by discrete beams with #MAT S08 material.

In the actual collision of a rail vehicle, the contact between the wheels and the track is a complex contact process dominated by rolling friction and supplemented by the Coulomb sliding friction. The rolling friction force is much small, but due to the existence of Coulomb sliding friction caused by the deformation of the wheel or the track, there is still a certain Coulomb sliding friction force between the wheel and rail when the wheels roll on the track. To bring the simulation model closer to the actual vehicle situation, it is necessary to introduce an equivalent Coulomb sliding friction coefficient in the wheel-rail contact.

It is very difficult to accurately measure the Coulomb sliding friction coefficient and the force between the wheel and the rail. In addition, the Coulomb sliding friction force and the coefficient are influenced by the condition of the track and environmental factors, e.g. if the track is covered with rain and snow, the equivalent Coulomb sliding friction coefficient becomes smaller. The equivalent Coulomb sliding friction coefficient between wheel and rail is considered as 0.008 in Ref. [19].

In this study, the wheel-rail contact force is simulated by discrete beams with #MAT S03 material and the equivalent friction coefficient is also considered as 0.008 referring to Ref. [19].

3.2 Model Validation
The BS EN 15227:2020 (E) standard [1] clearly clarifies that evaluating the behavior of a complete train by physical testing is impractical, but it could be validated by dynamic simulation. Also, in Refs. [16] and [19], FE
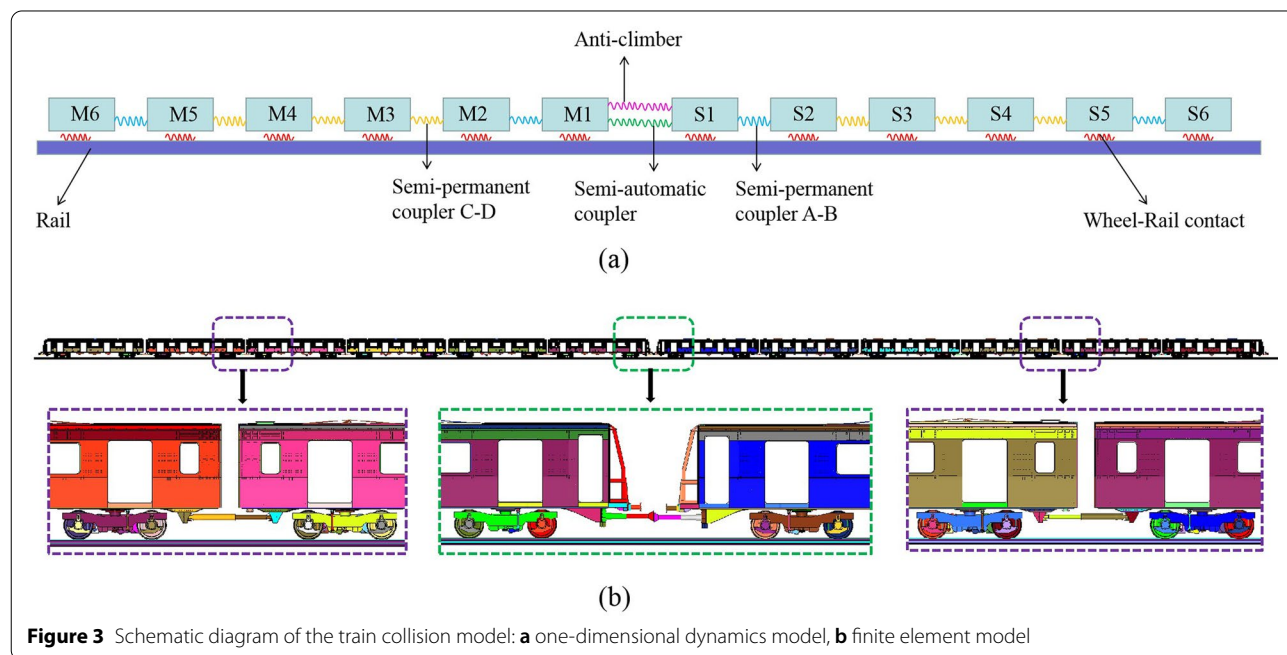

Figure 3 Schematic diagram of the train collision model: **a** one-dimensional dynamics model, **b** finite element model

Liu *et al. Chinese Journal of Mechanical Engineering*   (2022) 35:85

Page 5 of 18

Table 1 Comparison between the modeling methods used for the train collision models

Structure name	Modeling method	
	Dynamics model	**Finite element model**
Track	1. Hexahedral elements are applied. 2. #MAT 20 material is assigned. 3. All degrees of freedom are restricted.	1. Hexahedral elements are applied. 2. #MAT 20 material is assigned. 3. All degrees of freedom are restricted. 4. The actual rail profile is considered.
Carbody	1. Hexahedral elements are applied. 2. #MAT 20 material is assigned. 3. The translational freedom along with the train movement is retained and other degrees of freedom are restricted. 4. The material density is adjusted to achieve the weight change.	1. Mainly quadrilateral shell elements and triangular elements in local irregular locations are applied. 2. Hexahedral elements for structures with a thickness above 20 mm are defined. 3. The element size is controlled within 15–20 mm. 4. #MAT 24 elastoplastic material is assigned.
Bogie	1. The bogie is not modeled. 2. The equivalent weight is added to the carbody.	1. Quadrilateral shell elements are used. 2. The bogie-frame, wheel-set, axle box, gearbox, anti-rolling torsion bar, and traction rod seat are modeled separately. 3. #MAT 20 material is assigned; 4. Joint elements are added to simulate the relative motion among different parts; 5. Discrete beams are applied with #MAT 67 material to simulate the primary and secondary suspensions, considering the actual stiffness and damping.
Anti-climbing energy-absorbing device, semi-automatic and semi-permanent couplers	1. Discrete beams are applied with #MAT S08 material. 2. The corresponding curves in Figure 2 are considered as the input curves.	1. Quadrilateral shell elements are used for the structures and the #MAT 20 material is assigned. 2. Joint elements are added to simulate the relative motion between different parts. 3. Discrete beam elements are used with #MAT S08 material to simulate the mechanical characteristics, the corresponding curves in Figure 2 are considered as the input curves.
Wheel-rail contact	1. Discrete beam elements are applied with #MAT S03 material. 2. The equivalent friction force is input; the friction coefficient is considered as 0.008 [19].	1. Surface to surface contact between the wheel and rail is defined. 2. The friction coefficient is considered as 0.008 [19].
Vehicle contact	1, Contact between the vehicles is not considered.	1. Self-contact between the vehicles is defined. 2. The friction coefficient is considered as 0.15 [32].

models were used to verify the accuracy of the dynamics model. Thus, it is a feasible method to validate the dynamics model by applying the FE model when the physical test could not be conducted.

The train collision finite element model was established using the LS-DYNA software, as showed in Figure 3(b), and the detailed modeling method used for the FE model is shown in Table 1. The wheel-rail contact equivalent friction coefficient is also considered as 0.008 [19].

Different from the wheel-rail contacting, the contacts between the two colliding trains and the adjacent vehicles in the marshalling train during the collision process are completely the Coulomb sliding contacts, and there must be Coulomb sliding friction forces. The materials used for the vehicles are stainless steel. Ref. [32] gives the Coulomb sliding friction coefficients of common used materials and the equivalent Coulomb

sliding friction coefficient between the steel and the steel is 0.15 [32].

In order to better simulate the actual collision situation, the contacts between the impacting trains and adjacent vehicles are added in the three-dimensional train collision simulation model, and the equivalent Coulomb sliding friction coefficients are introduced to simulate the contact friction forces. Referring to Ref. [32], the equivalent Coulomb sliding friction coefficients are also taken as 0.15.

In Ref. [33], the accuracy of the one-dimensional train collision dynamics model has been verified by comparing the simulation results with the energy absorbing devices' test results and the three-dimensional train collision FE model's simulation results including the compression stroke of each collision interface, the train collision energy conversion and the vehicles' velocity versus time curves.

In this study, to further verify the accuracy of the one-dimensional train collision dynamics model, numerical calculations were performed on both the train collision models using the same boundary conditions, based on the two collision scenarios including different collision weight and collision speed, as shown in Table 2. The compression displacement of each collision interface, the energy collision conversion curves, and vehicles' velocity versus time curves were compared between the two models.

The comparison result of the train collision energy conversion between the collision models based on the collision scenario 1 is presented in Figure 4(a), based on the collision scenario 2 is presented in Figure 4(d). From Figure 4(a) and (d), it can be seen that in the train collision process, the kinetic energy decreases gradually and converts into the internal energy, the total energy keeps the same and finally the internal energy is about half of the initial kinetic energy. For both collision scenarios, the collision energy conversion curves between the train collision dynamics model and the finite element model are very consistent and the energy change trends and times are almost identical.

The comparison of the compression displacements of each collision interface for the two models in both two collision scenarios are shown in Figure 4(b) and (e). And it can be seen that the compression displacements of each collision interface of the two models have the same distribution, the S1-M1 collision interface between the two trains has the largest compression displacement, while the compression displacements of the other collision interfaces are symmetrically distributed around the S1-M1 collision interface and gradually decrease towards the two ends. The kinetic energy of the train collision is mainly absorbed by the energy absorbers located at the first three collision interfaces. The compression displacements of the two models are slightly different at the S1-M1, S2-S3 and M2-M3 collision interfaces, which

may be due to the elastic energy absorption of car-bodies in the FE model, while the other collision interfaces are essentially the same.

The comparison of the vehicles' velocity versus time curves of the two models in both two collision scenarios are shown in Figure 4(c) and (f). And it can be seen that similar to the energy conversion curves, the vehicles' velocity versus time curves of the two models also exhibit the same trend and balance time. After balance, the final vehicles' velocity is approximately half the initial velocity. Compared to the dynamics model, the final vehicles' velocity of the FE model is slightly lower, and the curves have higher fluctuates, which can be mainly attributed to the elastic energy absorption of the vehicles. In general, the two models show good agreement.

In summary, by comparing the dynamics model and the FE model from above two collision scenarios and three aspects, the one-dimensional train collision dynamics model always shows good consistency with the FE model. It can be proved that the calculation results of the one-dimensional train collision dynamics model are accurate and reliable, and the proposed model can be used as a basic model for further research.

4 Vehicle Design Parameters and Train Crashworthiness Criteria

4.1 Definition of Vehicle Design Parameters
It is assumed that the design collision weight (vehicle weight in work order plus half weight of the seated passengers) of each vehicle in the B-type train is the same, which is M. The vehicle design collision weight M, the train collision speed V, and the empty stroke D between the semi-automatic coupler and the anti-climber all have a significant influence on the train's collision response. The standard collision speed of a subway train is 25 km/h [1]. The vehicle design collision weight M and the empty stroke D are inherent design parameters of the vehicle and are not restricted by the standard. Thus, M and D

Table 2 Boundary conditions for the collision numerical calculation

Collision Scenario	Item	Boundary condition
1	Collision mass 1	The weight of the Tc car is 34.08 t, the weight of the Mp/M car is 36.26 t, and the total weight of the six-car marshaling train is 213.2 t.
	Collision velocity	25 km/h
	Wheel-rail friction	The wheel/rail friction coefficient is set as 0.008 [19].
2	Collision mass 2 (work order plus six persons standing per square meter)	The weight of the Tc car is 46.56 t, the weight of the Mp/M car is 50.24 t, and the total weight of the six-car marshaling train is 294.08 t.
	Collision velocity	15 km/h
	Wheel-rail friction	The wheel/rail friction coefficient is set as 0.008 [19].
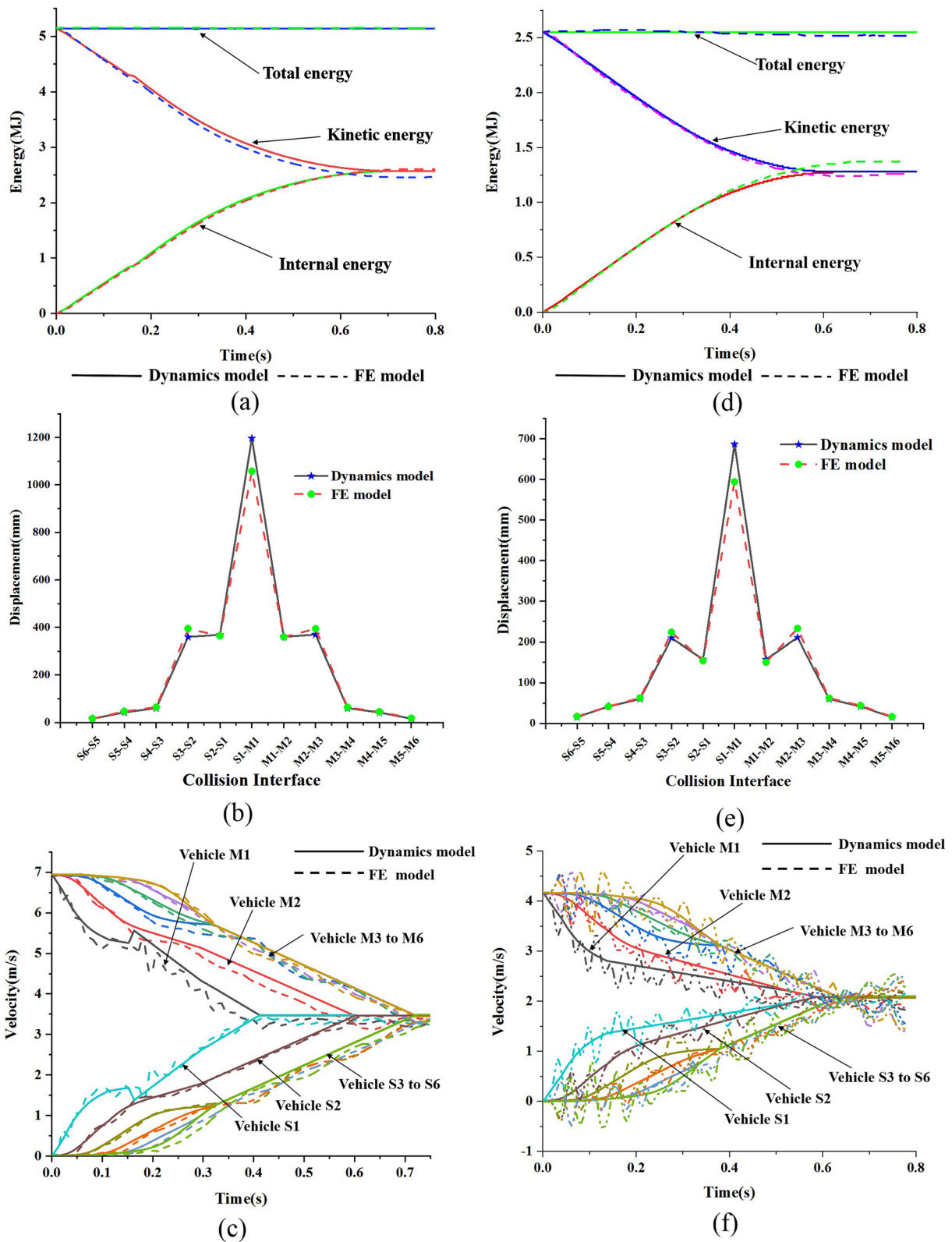
Figure 4 Comparison of the results between the MB and FE models: **a** Collision energy conversion for scenario 1, **b** Compression displacement of each collision interface for scenario 1, **c** Vehicles' velocity versus time curves for scenario 1, **d** Collision energy conversion for scenario 2, **e** Compression displacement of each collision interface for scenario 2, **f** Vehicles' velocity versus time curves for scenario 2

Liu *et al. Chinese Journal of Mechanical Engineering* (2022) 35:85

Page 8 of 18

are considered as the vehicle design variable parameters, and the corresponding range of values is: 30 t $\leq M \leq$ 36 t, 20 mm $\leq D \leq$ 50 mm.

4.2 Definition of Train Crashworthiness Evaluation Criteria

In Ref. [19], two comprehensive crashworthiness evaluation criteria have been proposed for the entire train, namely *TS* (total crash displacement along the train) and *TMA* (total mean acceleration along the train). The smaller is the *TS*, the higher is the integrity of the occupant's survival space; the smaller is the *TMA*, the lower is the train collision acceleration.

In this study, due to the symmetry of the collision response between the moving and stationary trains, only the moving train was considered. Furthermore, the maximum collision instantaneous acceleration was considered as the vehicle collision acceleration response. In this study, based on Ref. [19], *TS* and *TAMA* were selected as the train's crashworthiness evaluation criteria, and the definitions of *TS* and *TAMA* are shown in Eqs. (1) and (2).

The total compression displacement along the moving train, *TS*, is defined as:

$$TS = \sum_{j=1}^{n} S_j, \tag{1}$$

where *n* is the number of collision interfaces of the moving train, and S_i is the compression displacement of the energy-absorbing device at the collision interface *j* of the moving train.

The overall mean acceleration along the moving train, *TAMA*, can be defined as:

$$TAMA = \frac{\sum_{i=1}^{m} MA_i}{m}, \tag{2}$$

where MA_i is the maximum collision instantaneous acceleration of the vehicle *i* in the moving train, and *m* is the number of vehicles of the moving train.

5 Influence of the Empty Stroke *D* on Train Collision Response

The vehicle design collision weight *M* was fixed at 33 t, and the empty stroke *D* was taken nine points at equal intervals within the defined range. Under the standard subway train collision scenario [1], based on the numerical simulation results of the one-dimensional train collision dynamics model, the influence law of the empty stroke *D* on the train collision response was investigated.

5.1 Influence on the Response of the Energy-absorbing Device

Under different empty stroke *D* values, the compression displacement and energy absorption versus time curves of the energy-absorbing devices at each collision interface along the moving train are shown in Figure 5. And it can be seen that with increase in *D*, the compression displacement and energy absorption at the collision interface S1-M1 (anti-climbers) and M1-M2 generally show an upward trend, but are not strictly monotonous. In contrast, the compression displacement and energy absorption at the M2-M3 collision interface gradually decrease. The compression displacement and energy
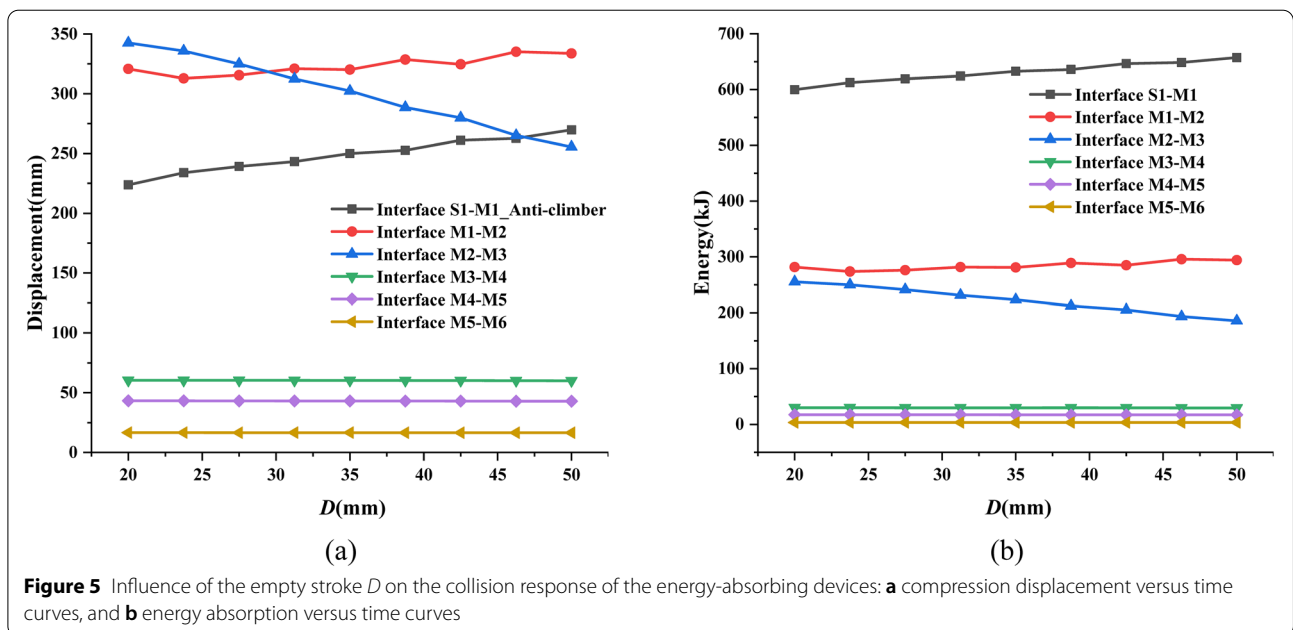

Figure 5 Influence of the empty stroke *D* on the collision response of the energy-absorbing devices: **a** compression displacement versus time curves, and **b** energy absorption versus time curves

Liu *et al. Chinese Journal of Mechanical Engineering*   (2022) 35:85

Page 9 of 18

absorption at the other three collision interfaces change slightly, and the curves are nearly horizontal.

Table 3 lists the compression displacement and energy absorption of the energy-absorbing devices located at the first three collision interfaces under different D values. It can be concluded from Table 3 that the semi-automatic coupler is always fully compressed and sheared off at the initial velocity of 25 km. With increase in D from 20 to 50 mm, compared to the initial value, the relative changes in the compression displacement at the first three collision interfaces are 20.59%, 4.03% and -25.41% respectively; furthermore, the relative changes in the energy absorption are 9.60%, 4.48% and -27.25% respectively.

While the empty stroke D has a significant impact on the compression displacement and energy absorption of the first three collision interfaces, it has little effect on the latter three collision interfaces. In general, D has a positive effect on the S1-M1 and M1-M2 collision interfaces, while it has a negative effect on the M2-M3 collision interface. Among the first three collision interfaces, D has the greatest effect on the M2-M3 collision interface, followed by S1-M1, and has the least effect on the M1-M2 interface. The empty stroke D exhibits the same influence laws on the compression displacement and energy absorption at different train collision interfaces.

5.2 Influence on the Vehicle Response

Under different empty stroke D, the velocity versus time curves of each vehicle of the moving train are shown in Figure 6. It can be seen from the figure that with increase in D, the velocity versus time curves of vehicles M1 and M2 begin to shift at 0.2 s. The velocity profiles at different D are shifted to parallel each other, and the time at which the final velocity reaches balance is also shifted. In contrast, the velocity curves of vehicles M3 to M6 remain the same under different D. With increase in D from 20 to 50 mm, the velocity balance times of vehicles M1 and M2 increase from 0.396 to 0.433 s and 0.556 to 0.595 s respectively.

Table 4 lists the maximum collision instantaneous acceleration of each vehicle of the moving train under different empty stroke D. It can be concluded that with increase in D, the maximum collision instantaneous acceleration of vehicles M1 to M3 remains the same; the maximum collision instantaneous acceleration of vehicles M4 to M6 shows a minor change compared to the initial value, and the relative changes are -0.47%, -1.16% and -0.11% respectively.

The maximum collision instantaneous acceleration of a vehicle is not directly affected by the empty stroke D, which is completely determined by the compression force of the energy-absorbing devices located at both ends of the vehicle and the vehicle's weight. A slight change in the maximum collision instantaneous acceleration of vehicles M3 to M6 is caused by the different compression displacements of the energy-absorbing devices located at both ends of the vehicle, which is within the range of the coupler buffer, and different compression displacements produce different compression forces.

5.3 Influence on the Responses of *TS* and *TAMA*

The collision responses of *TS* and *TAMA* under different D along the moving train are listed in Table 5. It is known that both *TS* and *TAMA* show a downward trend with increase in D. With increase in D from 20 to 50 mm, compared to the initial value, the relative changes in *TS* and *TAMA* are -2.11% and -0.22% respectively.

The empty stroke D has a negative impact on *TS* and *TAMA*. Similarly, D has no direct effect on *TAMA*. The decrease in *TAMA* can also be attributed to the slight

Table 3 Collision responses of the energy-absorbing devices under different empty stroke D

Empty stroke D(mm)	Compression displacement (mm)				Energy absorption (kJ)		
	Collision Interface S1-M1 Semi-automatic coupler	Collision Interface S1-M1 Anti-climbers	Collision Interface M1-M2	Collision Interface M2-M3	Collision Interface S1-M1	Collision Interface M1-M2	Collision Interface M2-M3
20	353	223.7	320.77	342.6	599.78	281.48	255.46
23.75	353	233.95	312.86	335.86	612.57	273.68	250.07
27.5	353	239.15	315.56	324.94	619.05	275.95	241.33
31.25	353	243.2	320.96	312.42	624.13	281.45	231.31
35	353	250	320.17	302.36	632.62	280.84	223.27
38.75	353	252.65	328.56	288.64	635.98	288.94	212.3
42.5	353	261.05	324.62	279.86	646.46	284.9	205.26
46.25	353	262.6	335.12	265.16	648.4	295.66	193.5
50	353	269.75	333.71	255.56	657.36	294.08	185.84
Relative change (%)	–	20.59	4.03	-25.41	9.60	4.48	-27.25

Figure 6 Velocity versus time curves of vehicles under different *D*
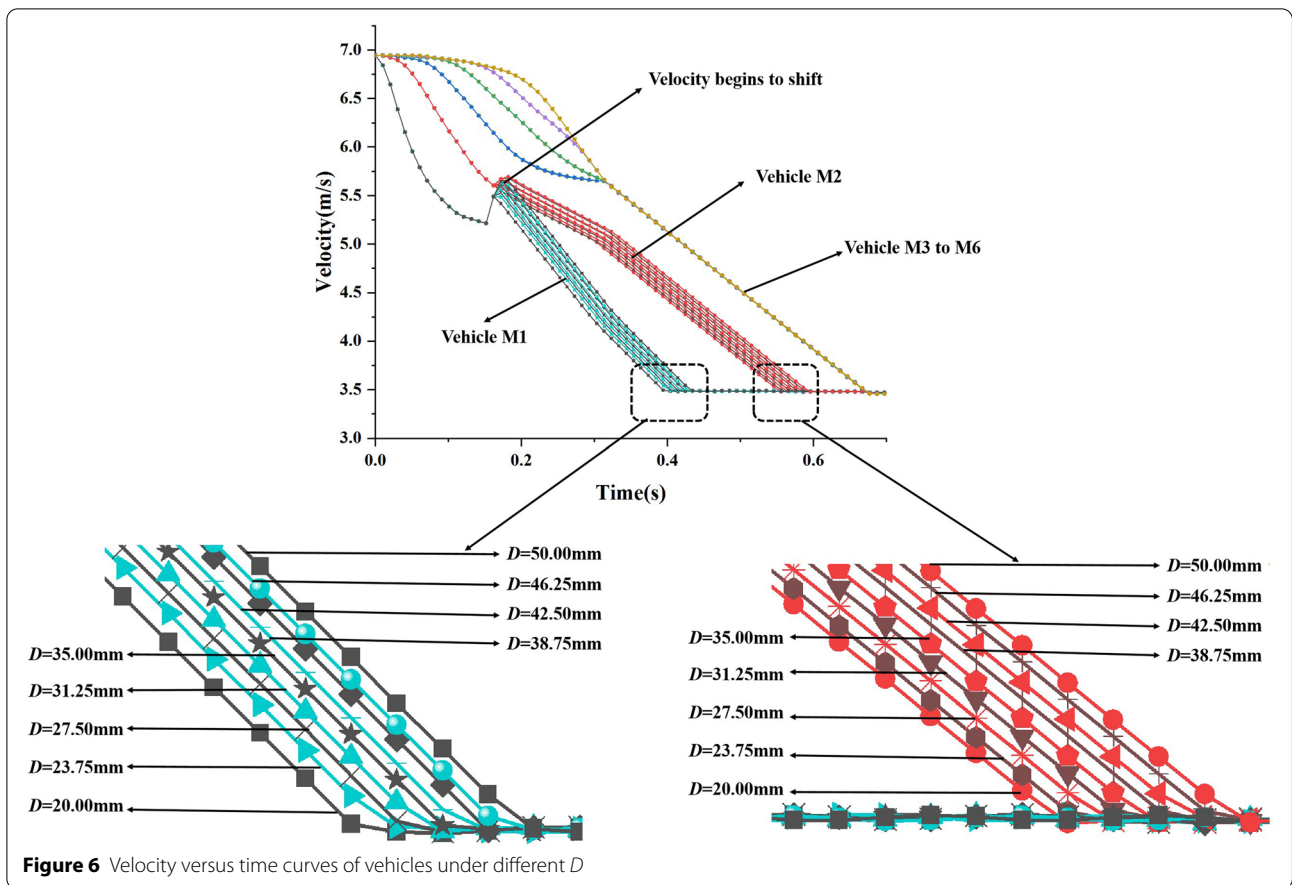
Table 4 Vehicle collision acceleration response under different *D*

Empty stroke *D*(mm)	Maximum collision instantaneous acceleration (g)					
	Vehicle M1	Vehicle M2	Vehicle M3	Vehicle M4	Vehicle M5	Vehicle M6
20	2.8739	1.3181	0.9199	0.7526	1.0643	1.1362
23.75	2.8739	1.3181	0.9199	0.7526	1.0643	1.1362
27.5	2.8739	1.3181	0.9199	0.7519	1.0582	1.1358
31.25	2.8739	1.3181	0.9199	0.7512	1.057	1.1357
35	2.8739	1.3181	0.9199	0.7509	1.0568	1.1355
38.75	2.8739	1.3181	0.9199	0.7504	1.0549	1.1351
42.5	2.8739	1.3181	0.9199	0.7503	1.055	1.1352
46.25	2.8739	1.3181	0.9199	0.7498	1.0532	1.1351
50	2.8739	1.3181	0.9199	0.7491	1.052	1.1349
Relative change (%)	0	0	0	− 0.47	− 1.16	− 0.11

change in the maximum collision instantaneous accelerations of vehicles M3 to M6.

6 Influence of the Vehicle Design Collision Weight *M* on Train Collision Response

The empty stroke *D* was fixed at 35 mm, and the vehicle design collision weight *M* was taken nine points at equal intervals within the defined range. Under the standard subway train collision scenario [1], based on

Table 5 Responses of *TS* and *TAMA* under different *D*

Empty stroke *D* (mm)	*TS* (mm)	*TAMA* (g)
20	1360.236	1.3442
23.75	1355.836	1.3442
27.5	1352.722	1.343
31.25	1349.562	1.3426
35	1345.454	1.3425
38.75	1342.633	1.3421
42.5	1338.285	1.3421
46.25	1335.462	1.3417
50	1331.535	1.3413
Relative change %	− 2.11	− 0.22

the numerical simulation results of the one-dimensional train collision dynamics model, the influence laws of the vehicle design collision weight *M* on the train collision response were investigated.
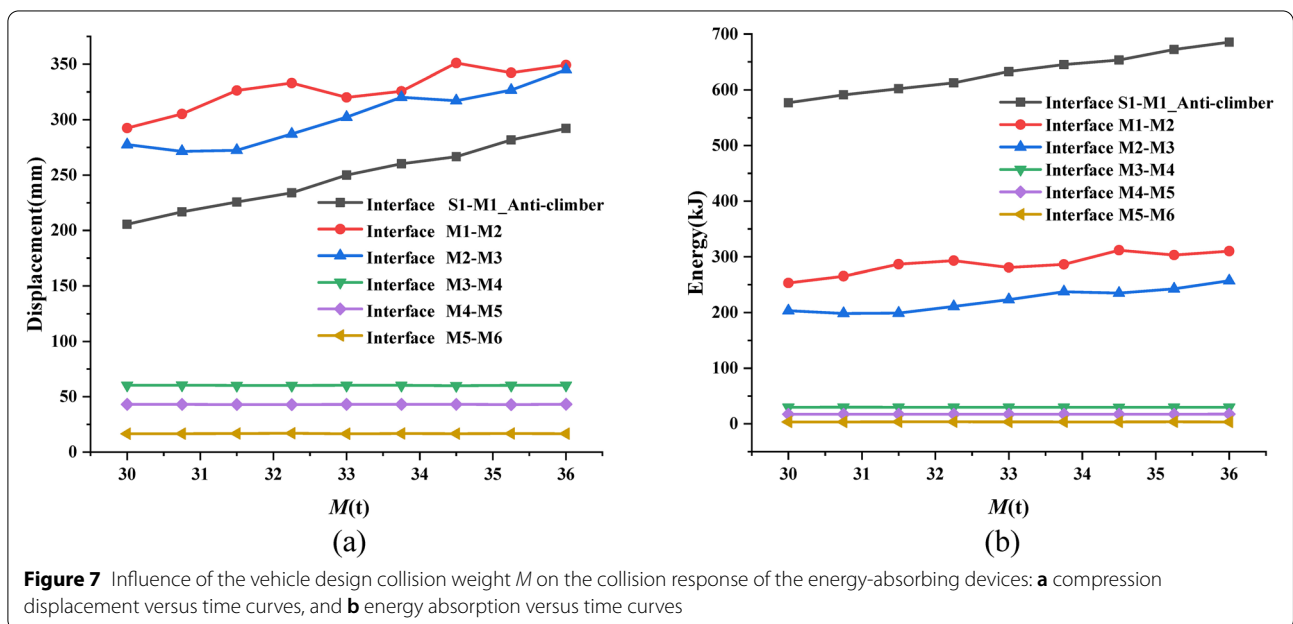
6.1 Influence on the Response of the Energy-absorbing Device

Under different vehicle design collision weights *M*, the compression displacement and energy absorption versus time curves of the energy-absorbing devices at each collision interface along the moving train are shown in Figure 7. And it can be observed that with an increase in *M*, the compression displacement and energy absorption at the collision interfaces S1-M1, M1-M2, and M2-M3 increase in general but are not strictly

monotonous. Similar to the situation under different *D*, the compression stroke and energy absorption at the other three collision interfaces change slightly, and the curves are almost horizontal.

Table 6 lists the compression displacement and energy absorption of the energy-absorbing devices located at the first three collision interfaces under different *M*. It can be seen from Table 6 that, in a similar manner, the semi-automatic coupler is always completely compressed and sheared off at the initial velocity of 25 km/h. With increase in *M* from 30 to 36 t, compared with the initial value, the relative changes in the compression displacement at the first three collision interfaces are 42.17%, 19.43% and 24.32% respectively; the relative changes in the energy absorption are 18.78%, 22.49% and 26.57% respectively.

The vehicle design collision weight *M* has a significant impact on the compression displacement and energy absorption of the first three collision interfaces, but has little effect on the latter three collision interfaces. In general, *M* has a positive effect on all the first three collision interfaces, in terms of the compression displacement and energy absorption. Considering the compression displacement, the impact on the S1-M1 collision interface is the greatest, followed by M2-M3, with the smallest impact on M1-M2. With respect to energy absorption, *M* has the greatest effect on the M2-M3 collision interface, followed by M1-M2, with the least effect on S1-M1.


Figure 7 Influence of the vehicle design collision weight *M* on the collision response of the energy-absorbing devices: **a** compression displacement versus time curves, and **b** energy absorption versus time curves

Table 6 Collision responses of the energy-absorbing devices under different vehicle design collision weights *M*

Vehicle designing weight *M* (t)	Compression displacement (mm)				Energy absorption (kJ)		
	Collision interface S1-M1 Semi-automatic coupler	Collision interface S1-M1 Anti-climbers	Collision interface M1-M2	Collision interface M2-M3	Collision interface S1-M1	Collision interface M1-M2	Collision interface M2-M3
30	353	205.5	292.43	277.48	576.99	253.19	203.36
30.75	353	216.75	305.15	271.47	591.05	265.31	198.53
31.5	353	225.7	326.45	272.37	602.23	286.73	199.25
32.25	353	233.95	333.08	287.18	612.57	293.23	211.13
33	353	250	320.17	302.36	632.62	280.84	223.27
33.75	353	260.15	325.62	320.21	645.31	286.47	237.57
34.5	353	266.6	350.97	317.13	653.37	311.76	235.07
35.25	353	281.7	342.35	326.71	672.25	303.12	242.74
36	353	292.15	349.24	344.95	685.33	310.13	257.4
Relative change (%)	–	42.17	19.43	24.32	18.78	22.49	26.57

6.2 Influence on the Vehicle Response

Under different vehicle design collision weights *M*, the velocity versus time curves of each vehicle of the moving train are shown in Figure 8. It can be seen from Figure 8 that with increase in *M*, the velocity versus time curves of all vehicles shift at the beginning of the train collision. Unlike the effect of the empty stroke *D*, the shifted velocity versus time curves are not parallel but gradually diverge, with the time at which the velocity eventually reaches balance also being shifted. With increase in *M*
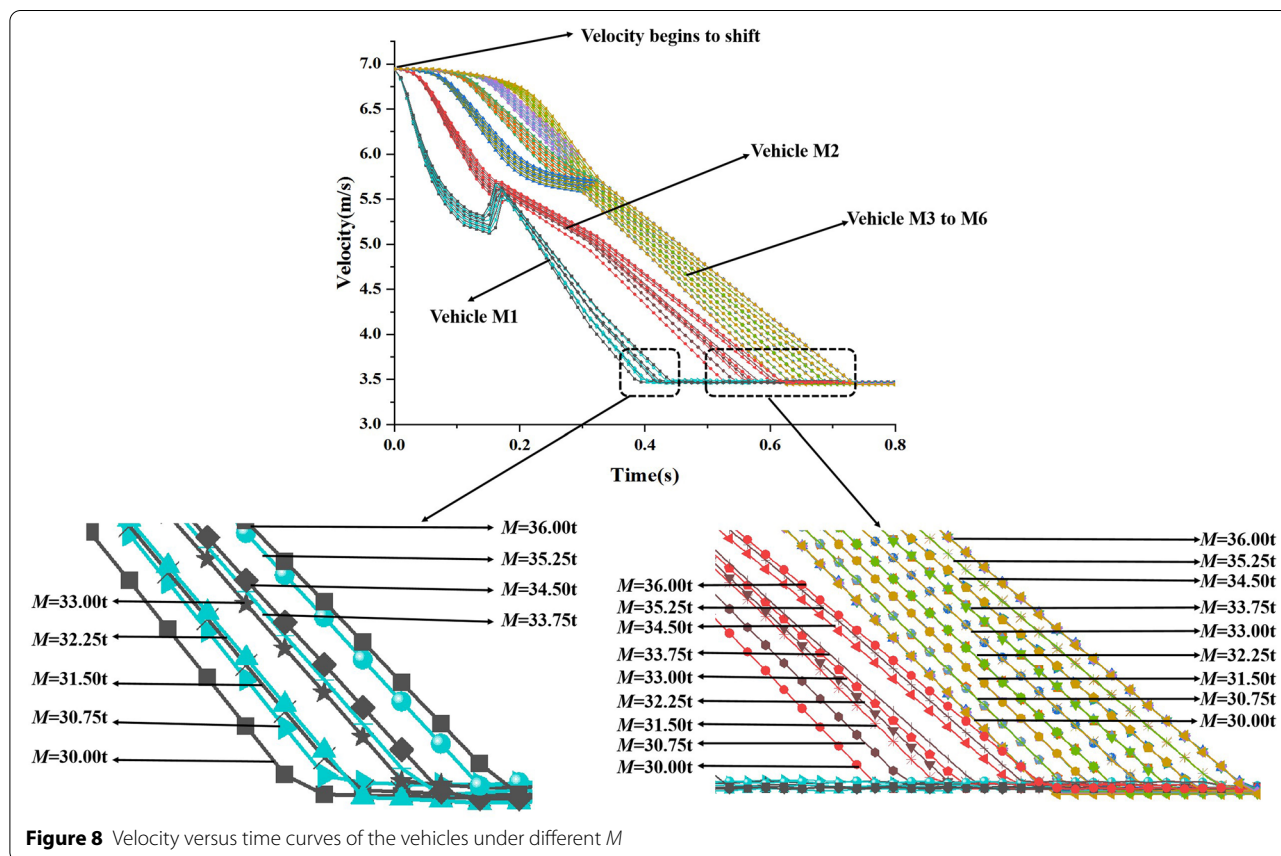
Figure 8 Velocity versus time curves of the vehicles under different *M*

Liu *et al. Chinese Journal of Mechanical Engineering*   (2022) 35:85

Page 13 of 18

Table 7 Vehicle collision acceleration response under different *M*

Vehicle designing weight *M* (t)	Maximum collision instantaneous acceleration (g)					
	Vehicle M1	Vehicle M2	Vehicle M3	Vehicle M4	Vehicle M5	Vehicle M6
30	3.1614	1.4469	1.0037	0.8259	1.1684	1.2459
30.75	3.0842	1.4126	0.9852	0.8016	1.1396	1.2201
31.5	3.0108	1.3797	0.9572	0.7903	1.112	1.1958
32.25	2.9407	1.3487	0.931	0.7579	1.0767	1.1789
33	2.8739	1.3181	0.9199	0.7509	1.0568	1.1355
33.75	2.8101	1.2891	0.8961	0.7327	1.0422	1.1156
34.5	2.749	1.2618	0.8718	0.7247	1.0204	1.0898
35.25	2.6905	1.2349	0.8543	0.6951	0.99	1.0721
36	2.6345	1.2087	0.8438	0.6893	0.9784	1.0415
Relative change (%)	− 16.67	− 16.46	− 15.93	− 16.54	− 16.26	− 16.41

from 30 to 36 t, the velocity balance times of vehicles M1 and M2 increase from 0.389 to 0.433 s and 0.53 to 0.621 s respectively; furthermore, the velocity balance times of vehicles M3 to M6 increase from 0.62 to 0.733 s.

Table 7 lists the maximum collision instantaneous accelerations of each vehicle in the moving train under different *M*. It can be seen that with increase in *M* from 30 to 36 t, the maximum collision instantaneous accelerations of all vehicles decrease linearly, and compared with the initial value, the relative changes are all around − 16%.

The vehicle design collision weight *M* directly determines the vehicles' maximum collision instantaneous acceleration. An increase in *M* leads to an extension of the balance time of the vehicle velocity, and therefore directly leads to a decrease in the average acceleration of the vehicle in the train collision.

6.3 Influence on the Responses of *TS* and *TAMA*

The collision responses of *TS* and *TAMA* under different *M* along the moving train are listed in Table 8. It is known that with increase in *M*, *TS* gradually increases, while *TAMA* gradually decreases. With an increase in *M* from 30 to 36 t, *TS* increases from 1248.459 to 1459.425 mm, indicating a relative change of 16.90%; *TAMA* decreases from 1.4422 to 1.2122 g, indicating a relative change of − 15.95%. *M* has a positive effect on the *TS*, while it has a negative effect on the *TAMA*.

7 Coupling Influence and Correlation Analysis of the Design Parameters

To investigate the coupling influence and correlation of *D* and *M* on the train collision responses, the OLHD method was applied to the experimental design within the defined range. Both *D* and *M* were selected as integers. The number of experiments was 10. In a standard subway train collision scenario (25 km/h), considering the compression displacements of the first three collision interfaces, the maximum collision instantaneous acceleration of the first two cars, and the responses of *TS* and *TAMA*, the one-dimensional train collision dynamics model was used for numerical simulation to obtain the train collision response matrix, as shown in Table 9.

The correlation coefficient is a statistical indicator that reflects the closeness of the relationship between variables, and the correlation coefficient ranges between − 1 and 1. If the correlation coefficient is 1, this indicates that the two variables are completely linearly correlated; − 1 indicates that the two variables are completely negatively correlated; 0 indicates that the two variables are not correlated. The closer the data is to 0, the weaker the correlation.

The correlation coefficient r_{xy} can be calculated as Eq. (3).

$$r_{xy} = \frac{s_{xy}}{s_x s_y}, \tag{3}$$

Table 8 Responses of *TS* and *TAMA* under different *M*

Vehicle designing weight *M* (t)	*TS* (mm)	*TAMA* (g)
30	1248.459	1.442
30.75	1266.546	1.409
31.5	1297.41	1.378
32.25	1327.219	1.344
33	1345.454	1.316
33.75	1378.996	1.290
34.5	1407.421	1.263
35.25	1423.718	1.234
36	1459.425	1.212
Relative change (%)	16.9	−15.95

Table 9 Train collision response matrix

Tests	Vehicle design parameters		Compression displacement (mm)			Maximum collision instantaneous acceleration (g)		TS(mm)	TAMA (g)
	D(mm)	M(t)	Collision interface S1-M1 Anti-climber	Collision interface M1-M2	Collision interface M2-M3	Vehicle M1	Vehicle M2		
1	20	35	243.95	363.90	363.58	3.07	1.22	1444.68	1.33
2	50	31	238.75	335.77	213.52	3.29	1.42	1260.95	1.47
3	37	32	233.05	332.46	276.86	3.18	1.45	1315.22	1.44
4	40	30	209.65	302.99	258.03	3.42	1.56	1243.66	1.54
5	23	33	231.9	314.43	337.22	3.15	1.29	1356.71	1.39
6	33	34	256.55	329.83	330.28	3.04	1.26	1389.72	1.34
7	43	35	282.15	365.24	302.94	2.91	1.3	1422.93	1.31
8	30	36	288.1	340.71	362.15	2.87	1.19	1464.29	1.27
9	47	33	263.55	335.85	262.78	3.08	1.38	1334.74	1.39
10	27	31	207.95	313.85	288.29	3.33	1.37	1283.35	1.47

where s_{xy} represents the sample covariance; s_x represents the sample standard deviation of x, and s_y represents the sample standard deviation of y.

The sample covariance and sample standard deviation can be calculated as Eqs. (4)–(6).

$$s_{xy} = \frac{\sum_{i=1}^{n} (x_i - \overline{x})(y - \overline{y})}{n - 1}, \tag{4}$$

$$s_x = \sqrt{\frac{\sum (x_i - \overline{x})^2}{n - 1}}, \tag{5}$$

$$s_y = \sqrt{\frac{\sum (y_i - \overline{y})^2}{n - 1}}, \tag{6}$$

where x_i is the sample ith value of x; $\overline{x}$ is the sample average value of x; y_i is the sample ith value of x; $\overline{y}$ is the sample average value of y, and n is the number of sample points.

The correlation coefficient matrix between the vehicle design parameters and train collision responses is shown in Table 10. It can be concluded that under the coupling effect of D and M, all responses show strong correlation with the vehicle design collision weight M. Among them, the compression displacement of the energy-absorbing devices located at the first three collision interfaces and TS are positively correlated, while the maximum collision instantaneous accelerations of vehicles M1 and M2 and $TAMA$ are negatively correlated.

The empty stroke D exhibits a positive correlation with the compression displacement of the collision interfaces S1-M1 and M1-M2, the maximum collision instantaneous accelerations of vehicles M1 to M2 and $TAMA$, while it shows negative correlations with the compression displacement of the collision interface M2-M3 and TS. The compression displacement at the collision interface M2-M3 and the maximum collision instantaneous acceleration of vehicle M2 are strongly correlated with D, while the other responses are weakly correlated with D.

8 Multi-objective Optimization and Decision Making

8.1 Formulation of the Surrogate Model
According to the train collision response matrix in Table 9, the surrogate models of TS and $TAMA$ are

Table 10 Correlation coefficient matrix

Vehicle design parameters	Energy-absorbing devices compression displacement			Vehicle maximum collision instantaneous acceleration		TS	TAMA
	Collision interface S1-M1 Anti-climber	Collision interface M1-M2	Collision interface M2-M3	Vehicle M1	Vehicle M2		
D	0.183	0.034	− 0.819	0.132	0.554	− 0.446	0.307
M	0.851	0.740	0.790	− 0.962	− 0.898	0.991	− 0.991

established based on the RSM, as shown in Eqs. (7) and (8).

$$TS = 4054.762 - 15.395D - 286.849M$$
$$+ 0.478D^2 + 9.307M^2 - 0.035DM \qquad (7)$$
$$- 0.005D^3 - 0.089M^3,$$

$$TAMA = -12.771 - 0.046D + 1.462M$$
$$- 0.002DM - 1.505e^{-5}D^3 \qquad (8)$$
$$+ 0.0005M^3.$$

To evaluate the accuracy of the obtained cubic polynomial surrogate models, three evaluation criteria are introduced, namely the average relative error (ARE), the root mean square error ($RSME$) and the fitting coefficient (R^2), as defined in Eqs. (9)–(11) [26, 27, 34, 35].

$$ARE = \frac{\sum \frac{|\hat{y}_i - y_i|}{y_i}}{n} \times 100\%, \qquad (9)$$

$$RSME = \sqrt{\frac{\sum_{i=1}^{n}(\hat{y}_i - y_i)^2}{n}}, \qquad (10)$$

$$R^2 = 1 - \frac{\sum(\hat{y}_i - y_i)^2}{\sum(\hat{y}_i - \bar{y}_i)^2}, \qquad (11)$$

where, y_i is the response predicted value of the surrogate model corresponding to each input variable experiment; y_i is the response value calculated from the train collision dynamics model corresponding to each input variable experiment, and y_i is the average response value calculated from the train collision dynamics model corresponding to all input variable experiments.

The results of the accuracy evaluation of the surrogate models are shown in Table 11. The closer the fit coefficient R^2 is to 1, the more accurate the surrogate model will be.

The smaller the sum, the better the accuracy of the surrogate model.

The smaller the ARE and $RSME$, the higher accuracy of the surrogate models. It can be concluded from Table 11 that the accuracy of the cubic polynomial surrogate

Table 11 Evaluation of the accuracy of the surrogate models

Accuracy evaluation criteria	*ARE*	*RSME*	*R²*
TS	0.066	0.073	0.952
TAMA	0.022	0.025	0.993

models established by the RSM is sufficiently high and can be used as basic models for further research.

8.2 Multi-objective Optimization
Based on the established surrogate models, under the standard subway train collision scenario (25 km/h), the particle swarm optimization algorithm (MOPSO) was applied to perform multi-objective optimization of *TS* and *TAMA*.

The empty stroke D and vehicle design collision weight M can be arbitrarily selected within the defined range, and the initial collision velocity of the train is considered to be 25 km/h. From Table 7, it can be seen that the maximum collision instantaneous acceleration of each vehicle is below 5 g, which meets the requirement of the standard [1]; therefore, the acceleration is no longer restricted. According to Figure 2, the maximum compression stroke of the anti-climber in S1-M1 interface S_{anti} is 265 mm, and the maximum compression stroke of the energy-absorbing devices at the other collision interfaces S_i ($i=1$–5) is 418 mm.

Based on the above objectives and constraints, the multi-objective optimization problem of the comprehensive train crashworthiness evaluation criteria *TS* and *TAMA* can be defined as Eq. (12).

$$\begin{cases} \text{Minimize} \\ TS(D,M), TAMA(D,M), \\ \qquad\qquad \text{s.t.} \\ 20\ \text{mm} \le D \le 50\ \text{mm}, \\ 30\ \text{t} \le M \le 36\ \text{t}, \\ V = 25\ \text{km/h}, \\ S_{anti} \le 265\ \text{mm}, \\ S_i(i=1-5) \le 418\ \text{mm}. \end{cases} \qquad (12)$$
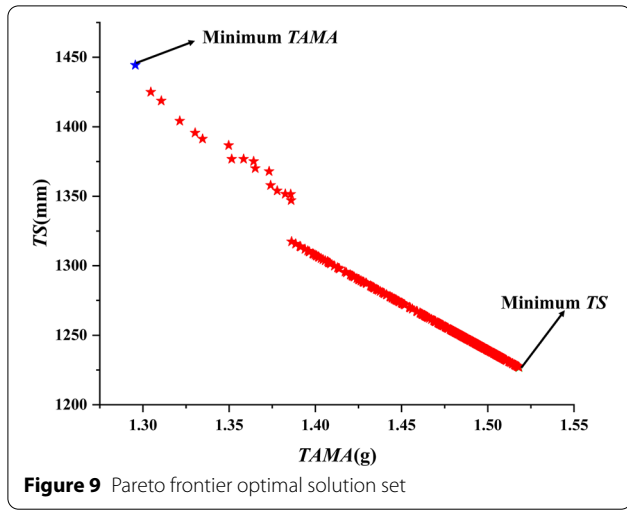
By optimizing and solving the multi-objective problem, the Pareto frontier optimal set of *TS* and *TAMA* can be obtained, as showed in Figure 9. And it can be seen that as *TS* decreasing, *TAMA* gradually increases. In contrast, as *TAMA* decreasing, *TS* gradually increases. The minimum *TS* can be derived from one end of the optimal set, while the minimum *TAMA* can be gained from the other end. *TS* and *TAMA* constitute a pair of relatively contradictory goals, which are consistent with the conclusion obtained in Ref. [19]. The values of *TS* and *TAMA* need to be determined according to the actual engineering requirements.

8.3 Multi-objective Decision Making
The entropy method is an objective weighting method. The entropy value can be used to measure the amount of data information contained in the evaluation criterion. The greater the data information contained in the

Liu *et al. Chinese Journal of Mechanical Engineering*   (2022) 35:85

Page 16 of 18

Figure 9 Pareto frontier optimal solution set

evaluation criterion, the smaller the entropy value [36, 37].

To minimize the influence on the evaluation results owing to the different dimensions and magnitude of the evaluation criteria, it is necessary to conduct dimensionless processing for each evaluation criterion [36]. In this study, a standardized approach [37] is employed, as defined in Eq. (13).

$$x_{ij}^* = \frac{x_{ij} - \overline{x}_j}{s_j}, \tag{13}$$

where $\overline{x}_j(j = 1, 2, 3, \cdots, m)$ is the average value of the observation of the item index j; $s_j(j = 1, 2, 3, \cdots, m)$ is the mean squared error of the observation of the item index j; x_{ij} and x_{ij}^* are the original and observation values obtained after standardized processing of the evaluation index j for the evaluated object i.

After standardized processing, the data may contain both positive and negative values, which are inconvenient for data processing. The T score function should be introduced to modify the standardized data [36, 38], as shown in Eq. (14).

$$x_{ij}^T = 10 \times x_{ij}^* + 50, \tag{14}$$

where x_{ij}^T is the transformed data.

The weighting factor calculation for the entropy method mainly consists of the following steps [37, 38]:

(1) Calculate the feature weight

$$p_{ij} = x_{ij}/\sum_{i=1}^{n} x_{ij}, \tag{15}$$

where P_{ij} is the characteristic proportion of the evaluated object (scheme) i under the evaluation criterion j.

(2) Calculate the entropy value of the evaluation criterion j

$$e_j = -\sum_{i=1}^{n} p_{ij} \ln(p_{ij}). \tag{16}$$

(3) Calculate the difference coefficient of the evaluation criterion j

$$g_j = 1 - e_j. \tag{17}$$

(4) Calculate the weight coefficient of the evaluation criterion j

$$w_j = g_j/\sum_{j=1}^{n} g_j \quad j = 1, 2, \cdots, m, \tag{18}$$

where the weight coefficient w_j is the weight of each evaluation criterion after normalization.

Using the entropy method, the weight coefficients of the train crashworthiness criteria are obtained, as shown in Table 12. The weight coefficients of *TS* and *TAMA* are 0.50003 and 0.49997 respectively.

The respective weight coefficients are assigned to *TS* and *TAMA*, and multi-objective optimization is performed by applying the MPOSO method to obtain the optimal solution, as shown in Table 13. It is known that when the empty stroke *D* is 50 mm, and the vehicle design collision weight *M* is 32.4 t, the optimal solution can be obtained. Here, *TS* is 1307.5 mm, and *TAMA* is 1.4 g.

Based on the same design parameters, the one-dimensional train collision dynamics model is used for the numerical calculations to obtain *TS* and *TAMA*. Compared with the predictions of the surrogate models, the

Table 12 Weight coefficients of the crashworthiness evaluation criteria

Crashworthiness criterion	Entropy value	Difference coefficient	Weight coefficient
TS	2.30111	− 1.30111	0.50003
TAMA	2.30093	− 1.30093	0.49997

Table 13 Multi-objective optimal solution under the entropy weight coefficient

Calculation method	*D*(mm)	*M* (t)	*TS* (mm)	*TAMA* (g)
Surrogate model	50	32.4	1307.5	1.4
Collision dynamics model	50	32.4	1318.96	1.36
Relative error (%)	−	−	0.87	3.01

relative errors of *TS* and *TAMA* are 0.87% and 3.01% respectively. This further validates the accuracy of the one-dimensional train collision dynamics model.

9 Discussion and Conclusion

Based on the one-dimensional collision dynamics model, the influence laws of the vehicle design collision weight *M* and empty stroke *D* on the train collision responses were investigated, multi-objective optimization and decision making were applied for minimizing both *TS* and *TAMA*. The main conclusions of this study are as follows.

(1) The empty stroke *D* has a significant impact on the compression displacement and energy absorption of the first three collision interfaces but has little effect on the latter three collision interfaces. In general, *D* has a positive effect on the S1-M1 and M1-M2 collision interfaces, while it has a negative impact on the M2-M3 collision interface. The velocity curves of vehicles M1 and M2 under different *D* are shifted and parallel to each other. With increase in *D* from 20 mm to 50 mm, the velocity balance times of vehicles M1 and M2 increase from 0.396 to 0.433 s and 0.556 to 0.595 s respectively. *D* has little effect on the maximum collision instantaneous accelerations of the vehicles. *D* has no direct influence on *TAMA*, although it exhibits a negative impact on *TS* and *TAMA*.

(2) Similar to *D*, the vehicle design collision weight *M* has a significant impact on the compression displacement and energy absorption of the first three collision interfaces, but has little effect on the latter three collision interfaces. In general, *M* has a positive effect on all of the first three collision interfaces. The velocity curves of all vehicles under different *M* are shifted and gradually divergent. With increase in *M* from 30 to 36 t, the velocity balance times of vehicles M1 and M2 increase from 0.389 to 0.433 s and 0.53 to 0.621 s respectively; furthermore, the velocity balance times of vehicles M3 to M6 increase from 0.62 to 0.733 s. *M* directly determines the maximum collision instantaneous acceleration of the vehicle, which decreases linearly as *M* increases. *M* has a positive effect on *TS*, while it has a negative effect on *TAMA*.

(3) Under the coupling effect of *D* and *M*, considering the responses of the compression displacements of the first three collision interfaces, the maximum collision instantaneous accelerations of the first two vehicles, *TS* and *TAMA*, all responses are strongly correlated with *M*. The compression displacement at the collision interface M2-M3 and the maximum collision instantaneous acceleration of vehicle M2 are strongly correlated with *D*, while all other responses are weakly correlated with *D*.

(4) After multi-objective optimization of *TS* and *TAMA* and multi-objective decision making based on the entropy method, the optimized comprehensive crashworthiness criteria were significantly improved. This study provides further theoretical and engineering application references for the design of subway train crashworthiness.

In this study, the influence laws on the train collision responses were investigated based on the range definition 30 t $\leq M \leq$ 36 t, 20 mm $\leq D \leq$ 50 mm, and $V = 25$ km/h. It is also assumed that all vehicles have the same weight, which is not the case for actual trains. When the vehicle design parameters and train collision speed are outside the range defined in this study, as well as different weights of vehicles, whether the effect laws on the train collision responses are consistent with the conclusions of this study needs further verification, which is the direction and focus of future research work.

Author contributions
YL: investigation, conceptualization, methodology, software, writing-original draft, data curation; formal analysis. BY: investigation, resources, writing-editing. SX: investigation, supervision, resources, funding acquisition, writing-review and editing, project administration. TZ: investigation, methodology, resources, funding acquisition, writing-editing. GY: review and editing, resources; supervision. RX: investigation, formal analysis. All authors read and approved the final manuscript.

Authors' Information
Yanwen Liu, born in 1988, is currently a PhD candidate at the *State Key Laboratory of Traction Power, Southwest Jiaotong University, China*. He research interests include passive safety of the railway vehicles.
Bing Yang, born in 1979, is currently a professor at *State Key Laboratory of Traction Power, Southwest Jiaotong University, China*. He received his PhD degree from *Southwest Jiaotong University, China,* in 2011. His research interests include structural strength and fatigue reliability.
Shoune Xiao, born in 1964, is currently a professor at *State Key Laboratory of Traction Power, Southwest Jiaotong University, China*. He received his master degree from *Southwest Jiaotong University, China*, in 1988. His research interests include vehicle dynamics, collision, structural strength and fatigue reliability.
Tao Zhu, born in 1984, is currently an associate professor at *State Key Laboratory of Traction Power, Southwest Jiaotong University, China*. He received his PhD degree from *Southwest Jiaotong University, China,* in 2012. His research interests include vehicle dynamics and train collision.
Guangwu Yang, born in 1977, is currently a professor at *State Key Laboratory of Traction Power, Southwest Jiaotong University, China*. He received his PhD degree from *Southwest Jiaotong University, China,* in 2005. His research interests include vehicle dynamics, vibration, and fatigue reliability.
Ruixian Xiu, born in 1987, is currently a lecturer at *College of Engineering, Changchun Normal University, China*. She received her master degree from *Southwest Jiaotong University, China*, in 2013. Her research interests include structural strength and fatigue reliability.

Author Details
[1] State Key Laboratory of Traction Power, Southwest Jiaotong University, Chengdu 610031, China. [2] Basic R&D Department, National Railway Passenger Car Engineering Research Center, Changchun Railway Vehicles Co., Ltd, Changchun 130113, China. [3] College of Engineering, Changchun Normal University, Changchun 130032, China.

References

[1] European Committee for Standardization. BS EN 15227: 2020 (E) Railway applications–Crashworthiness requirements for railway vehicle bodies. Brussels: CEN-CENELEC Management Center, 2020.

[2] The American Society of Mechanical Engineers. ASME RT-1-2015 Safety Standard for Structural Requirements for Light Rail Vehicles. New York: The American Society of Mechanical Engineers, 2015.

[3] The American Society of Mechanical Engineers. ASME RT-2-2014 Safety Standard for Structural Requirements for Heavy Rail Transit Vehicles. New York: The American Society of Mechanical Engineers, 2014.

[4] Y Yu, G J Gao, W Y Guan, et al. Scale similitude rules with acceleration consistency for trains collision. *Proc IMechE Part F: J Rail and Rapid Transit*, 2018, 232(10): 2466–2480.

[5] X D Xue, M Robinson, F Schmid, et al. Development issues for impact safety of rail vehicles:Robustness of crashworthy designs, effect of structural crashworthiness on passenger safety and behaviour characterisation of vehicle materials. *Proc IMechE Part F: J Rail and Rapid Transit*, 2018, 232(2): 461–470.

[6] L Xia, W G Liu, X J Lv, et al. A system methodology for optimization design of the structural crashworthiness of a vehicle subjected to a high speed frontal crash. *Engineering Optimization*, 2018, 50(4): 634–650.

[7] G Lu. Energy absorption requirement for crashworthy vehicles. *Proc IMechE Part F: J Rail and Rapid Transit*, 2002, 216(1): 31–39.

[8] A Scholes, J H Lewis. Development of crashworthiness for railway vehicle structures. *Proc IMechE, Part F: J Rail and Rapid Transit*, 1993, 207: 1–16.

[9] M Avalle, G Chiandussi. Optimisation of a vehicle energy absorbing steel component with experimental validation. *International Journal of Impact Engineering*, 2006, 34: 843–858.

[10] H Shao, P Xu, S G Yao, et al. Improved multibody dynamics for investigating energy dissipation in train collisions based on scaling laws. *Shock and Vibration*, 2016: 1–11.

[11] S Salehghaffari, M Rais-Rohani, A Najaf. Analysis and optimization of externally stiffened crush tubes. *Thin-Walled Structures*, 2011, 49: 397–408.

[12] S C Xie, X J Du, H Zhou, et al. Analysis of the crashworthiness design and collision dynamics of a subway train. *Proc IMechE Part F: J Rail and Rapid Transit*, 2020, 234(10): 1117–1128.

[13] T Zhu, S N Xiao, G Z Hu, et al. Crashworthiness analysis of the structure of metro vehicles constructed from typical materials and the lumped parameter model of frontal impact. *Transport*, 2019, 34(1): 75–88.

[14] T Zhu, S J Liu, S N Xiao, et al. Train collision dynamic model considering longitudinal and vertical coupling. *Advances in Mechanical Engineering*, 2019, 11(1): 1–9.

[15] J P Dias, M S Pereira. Optimization methods for crashworthiness design using multibody models. *Computers and Structures*, 2004, 82: 1371–1380.

[16] J F Milho, J A C Ambrósio, M F O S Pereira. Validated multibody model for train crash analysis. *International Journal of Crashworthiness*, 2003, 8(4): 339–352.

[17] C Yang, Q Li, S N Xiao, et al. On the overriding issue of train front end collision in rail vehicle dynamics. *Vehicle System Dynamics*, 2018, 56(4): 506–528.

[18] G Lu. Collision behaviour of crashworthy vehicles in rakes. *Proc IMechE Part F: J Rail and Rapid Transit*, 1999, 213(3): 143–160.

[19] H Zhao, P Xu, S H Jiang, et al. A novel design method of the impact zone of a high-speed train. *International Journal of Crashworthiness*, 2020: 1-10. https://doi.org/10.1080/13588265.2020.1808755.

[20] W L Yang, S C Xie, H H Li, et al. Design and injury analysis of the seated occupant protection posture in train collision. *Safety Science*, 2019, 117: 263–275.

[21] L Wei, L L Zhang. Evaluation and improvement of crashworthiness for high-speed train seats. *International Journal of Crashworthiness*, 2018, 23(5): 561–568.

[22] A Hault-Dubrulle, F Robache, P Drazetic, et al. Analysis of train driver protection in rail collisions: Part II. Design of a desk with improved crashworthiness performance. *International Journal of Crashworthiness*, 2013, 18(2): 194–205.

[23] H C Zhou, J Zhan, W B Wang, et al. Dynamic simulation of train driver under secondary impact. *Advances in Mechanical Engineering*, 2017, 9(12): 1–10.

[24] Y Peng, L Hou, M Z Yang, et al. Investigation of the train driver injuries and the optimization design of driver workspace during a collision. *Proc IMechE Part F: J Rail and Rapid Transit*, 2017, 231(8): 902–915.

[25] Z X Li, W Ma, S G Yao, et al. Crashworthiness performance of corrugation-reinforced multicell tubular structures. *International Journal of Mechanical Sciences*, 2021: 190. https://doi.org/10.1016/j.ijmecsci.2020.106038.

[26] S M Wang, Y Peng, T T Wang, et al. Collision performance and multi-objective robust optimization of a combined multi-cell thin-walled structure for high speed train. *Thin-Walled Structures*, 2019, 135: 341–355.

[27] J Y Wang, Z J Lu, M Zhong, et al. Coupled thermal-structural analysis and multi-objective optimization of a cutting-type energy-absorbing structure for subway vehicles. *Thin-Walled Structures*, 2019, 141: 360–373.

[28] C F Shu, S Y Zhao, S J Hou. Crashworthiness analysis of two-layered corrugated sandwich panels under crushing loading. *Thin-Walled Structures*, 2018, 133: 42–51.

[29] P Xu, C X Yang, Y Peng, et al. Cut-out grooves optimization to improve crashworthiness of a gradual energy-absorbing structure for subway vehicles. *Materials and Design*, 2016, 103: 132–143.

[30] P Xu, J Xing, S G Yao, et al. Energy distribution analysis and multi-objective optimization of a gradual energy-absorbing structure for subway vehicles. *Thin-Walled Structures*, 2017, 115: 255–263.

[31] L Wang, B H Li, C L Li, et al. Influence of collision energy absorption in no-acted stroke of train crash energy absorption system. *Journal of Dalian Jiaotong University*, 2019, 40(2): 16-19. (in Chinese)

[32] Department of Theoretical Mechanics, Harbin Institute of Technology. Theoretical Mechanics (I). Beijing: High Education Press, 2002. (in Chinese)

[33] Y W Liu, B Yang, S N Xiao, et al. Parameter study and multi-objective optimization for crashworthiness of a B-type metro train. *Proc IMechE Part F: J Rail and Rapid Transit*, 2021: 1-18. https://doi.org/10.1177/0954409721 1008283.

[34] Y K Sui, H P Yu. The improvement of response surface method and its application to engineering optimization. Beijing: Science Press, 2010. (in Chinese)

[35] Meituan Algorithm Team. Meituan machine learning practice. Beijing: People Post Press, 2018. (in Chinese)

[36] J K Zhang, T Zhu, X R Wang, et al. Comprehensive evaluation model for one-dimensional crash energy management of trains. *Journal of Southwest Jiaotong University*, 2021, 56(6): 1329-1336. (in Chinese)

[37] Y J Guo. Comprehensive evaluation theory, method and application [M]. Beijing: Science Press, 2007: 16–17; 45–47. (in Chinese)

[38] J Y Yu, X H He. Data statistical analysis and SPSS application. Beijing: People's Posts and Telecommunications Press, 2003. (in Chinese)